Supporting Information

Xue Li,[a] Ziqi Ma,[a] Yin Liu,[a] Xinqi Xu,[b] Rui Shi,[a] Qiang Wang,[d] Te Ba,[d] Chang Wei Kang,[d]Shengli Zhu,[a, c] Zhenduo Cui,[a] Zhaoyang Li,[a] Wence Xu,[a] Zhonghui Gao,[a] Jiamin Zhu,[a] Yanqin Liang,*[a] and Hui Jiang*[a, c]

1. Experimental Section

Chemicals and Reagents.

Trans-Stilbene (TSB, 98%) was purchased from Tianjin Heowns Opde Technology Co., Ltd. Diindenoperylene (DIP, 97%) was purchased from Shanghai Bide Pharmatech Ltd. Perylene (PER) (98%) was purchased from Pursuit (Tianjin) Biomedical Technology Co., Ltd. 2,6-Diphenylanthracene (2,6-DPA, 98%) and 9,10-diphenylanthracene (9,10-DPA, 98%) were purchased from Shanghai Macklin Biochemical Technology Co., Ltd. Trichloromethane (HPLC grade) was purchased from Tianjin Jiangtian Chemical Technology Co., Ltd. Bismuth germanate (BGO, 99.9995%) and polysulfone (PSF, 98%) were purchased from Shanghai Macklin Biochemical Technology Co., Ltd. TSB, DIP, PER, 2,6-DPA, and 9,10-DPA were purified by triple sublimation via the physical vapor transport (PVT) method. The remaining chemicals were used as received, without further purification.

Characterization Methods.

Macroscopic morphology of all crystalline samples was documented using a Sony digital camera. X-ray diffraction analysis was performed on a DX-2700BH diffractometer (Cu Kα radiation, $\lambda = 1.54056$ Å) over a 2θ range of 10–40°, with a scan step of 0.02° and a step time of 0.2 s, using a single-crystal silicon wafer as the substrate. Solid-state UV-Vis absorption spectra were collected on a Shimadzu UV-2700 spectrometer over 300–800 nm, with $BaSO_4$ powder as the reflectance background. Steady-state photoluminescence spectra were acquired using an Edinburgh FLS1000 spectrometer equipped with a Peltier-cooled Hamamatsu R928-P photomultiplier tube (detection range: 200-900 nm) and a 450 W xenon lamp excitation source. Luminescence decay kinetics were measured on the same spectrometer using a 375 nm pulsed laser as the excitation source. Photoluminescence quantum yield measurements were also carried out on this system. Infrared spectroscopy data were obtained using a Thermo Scientific Nicolet iS10 Fourier-transform infrared spectrometer over the wavenumber range of 400–4000 cm^{-1}. Radioluminescence spectra were collected using a commercial miniature X-ray source (silver target, maximum output: 200 μA/4 W) coupled with an Edinburgh FS5 fluorescence spectrophotometer. X-ray imaging experiments were conducted by combining a Canon EOS 700D camera with a tungsten-target X-ray tube, where the scintillator film was placed between the sample and the X-ray source, and images

were captured with an exposure time of 5 seconds. The X-ray source was operated at 50 kV and 80 μA, with an approximate distance of 20 cm between the source and the sample during imaging.

Theoretical Calculations.

Theoretical calculations were performed using the Gaussian 16 software package. The structural optimization of the highest occupied molecular orbital (HOMO) and lowest unoccupied molecular orbital (LUMO) energy levels for all molecules was conducted at the B3lyp/6-311+G (d, p) basis set level, and the corresponding molecular orbital diagrams were plotted using the wavefunction analysis tool Multiwfn.

2. Figures and Tables

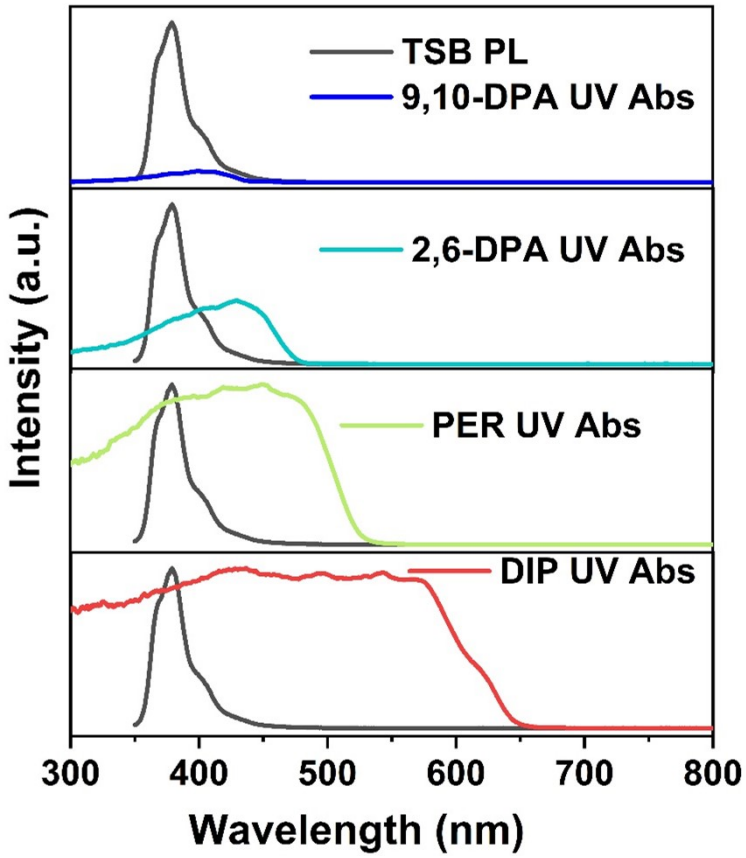

Figure S1. The overlap between the absorbance of dopants and the PL of TSB.

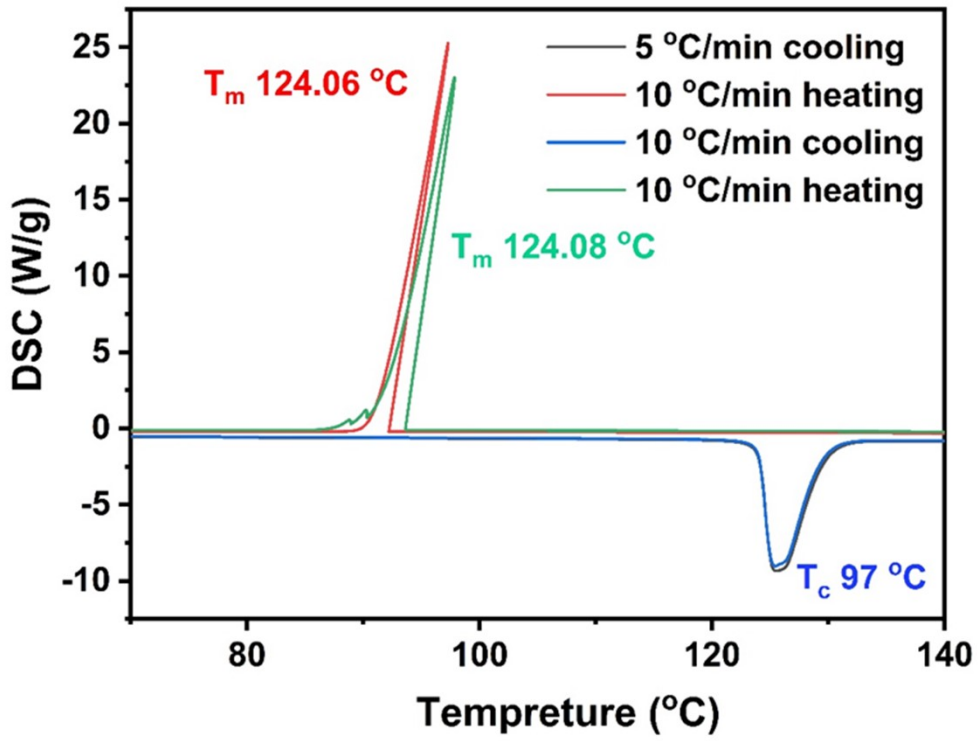

Figure S2. Differential scanning calorimetry test (DSC) of TSB.

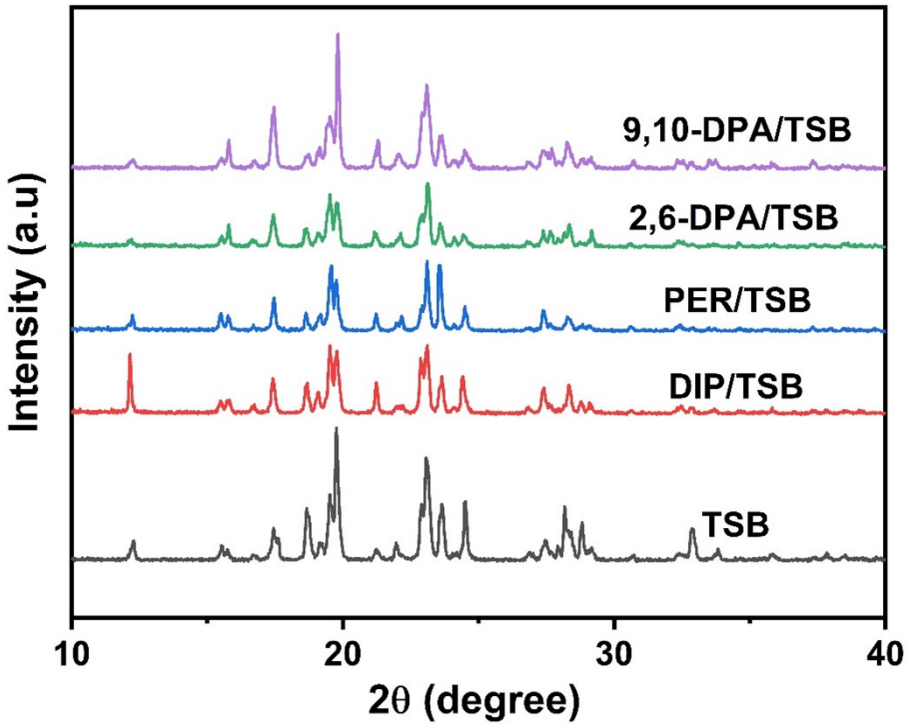

Figure S3. Powder X-ray diffraction patterns of TSB, DIP/TSB, PER/TSB, 2,6-DPA/TSB, and 9,10-DPA/TSB crystalline powders.

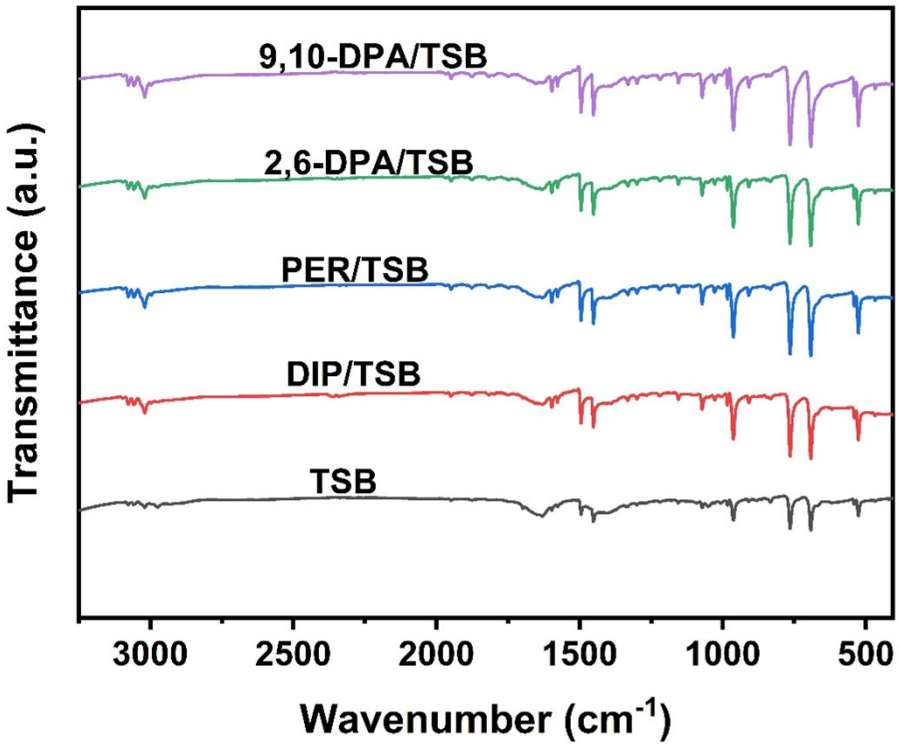

Figure S4. Fourier-transform infrared spectroscopy (FTIR) spectra of TSB, DIP/TSB, PER/TSB, 2,6-DPA/TSB, and 9,10-DPA/TSB crystals.

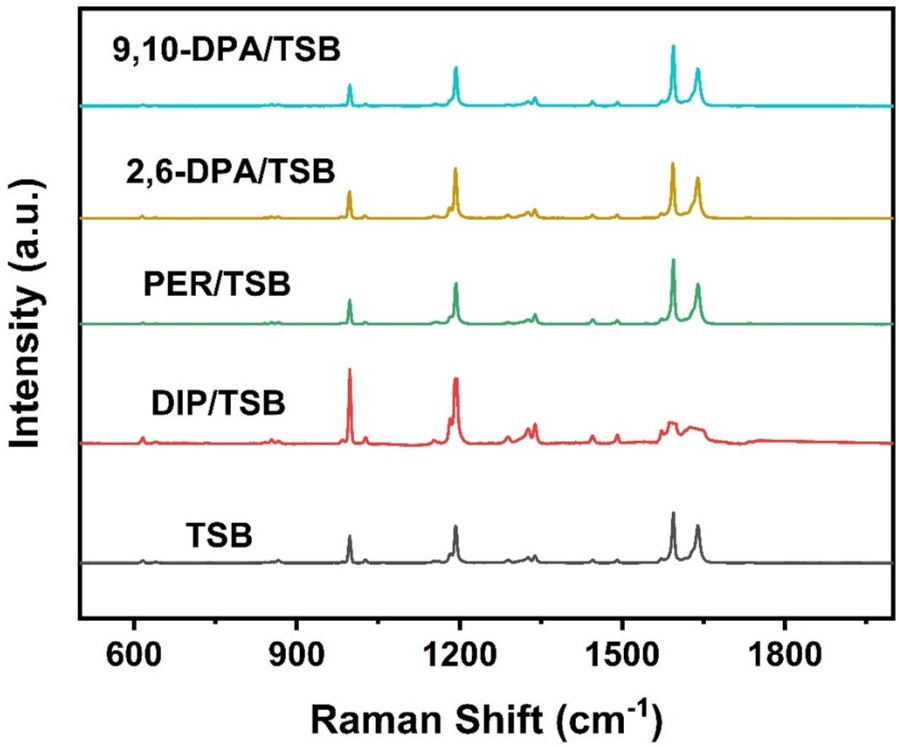

Figure S5. Laser Raman spectra of TSB, DIP/TSB, PER/TSB, 2,6-DPA/TSB, and 9,10-DPA/TSB crystals.

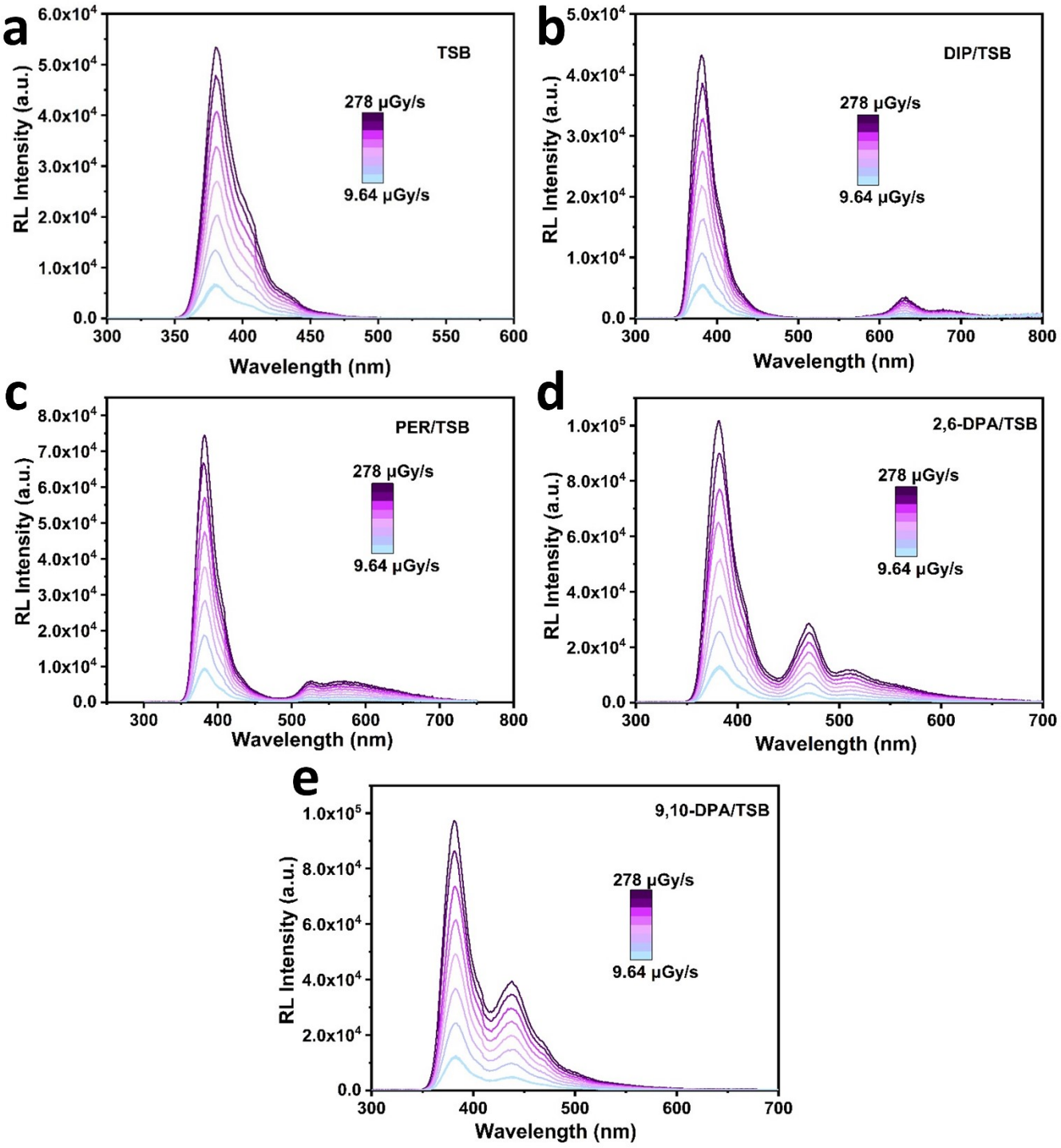

Figure S6. The RL intensity of TSB, DIP/TSB, PER/TSB, 2,6-DPA/TSB, and 9,10-DPA/TSB powders under the X-ray dose rate range from 9.64 to 278 μGy s^{-1}, respectively.

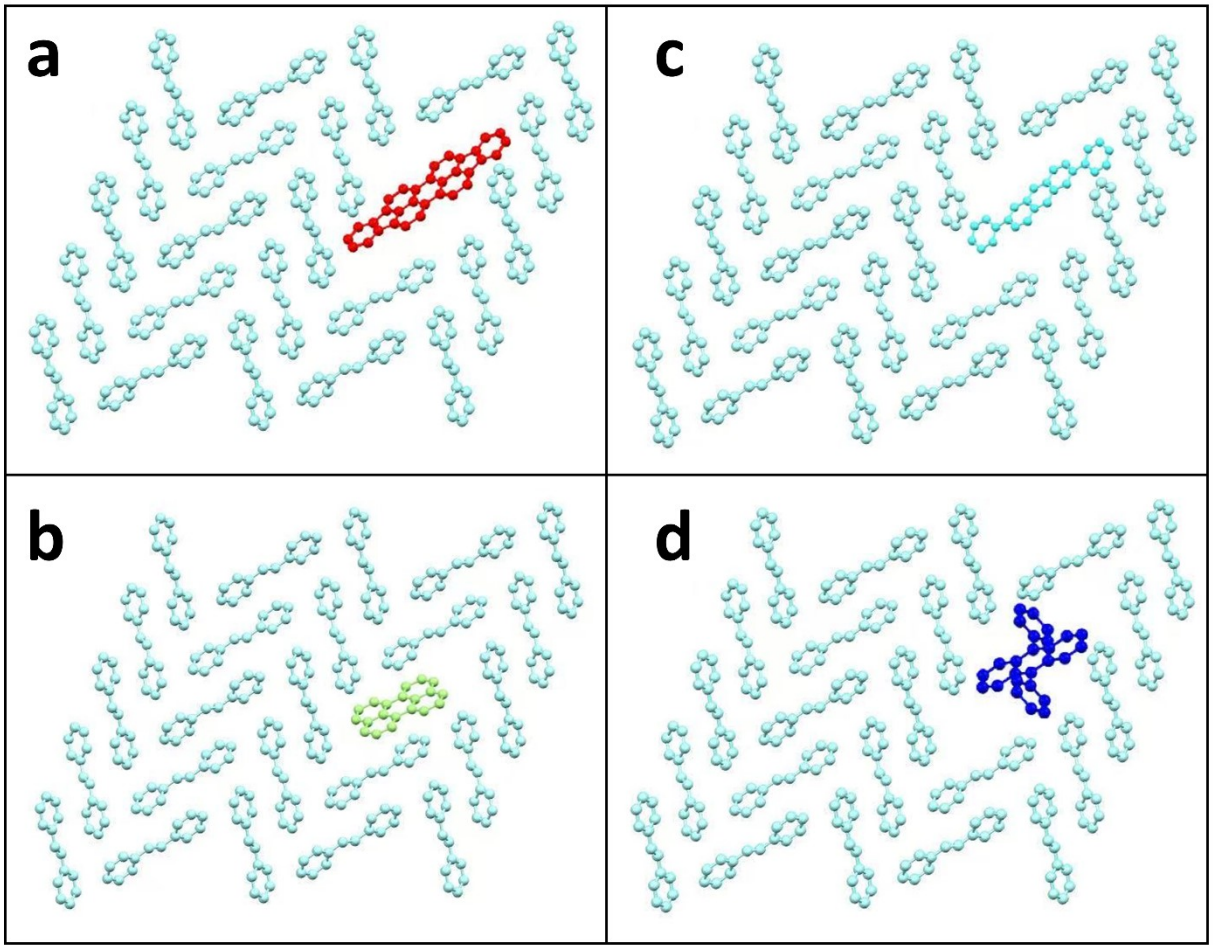

Figure S7. Simulated packing diagrams of (a) DIP/TSB, (b) PER/TSB, (c) 2,6-DPA/TSB, and (d) 9,10-DPA/TSB doped crystals.

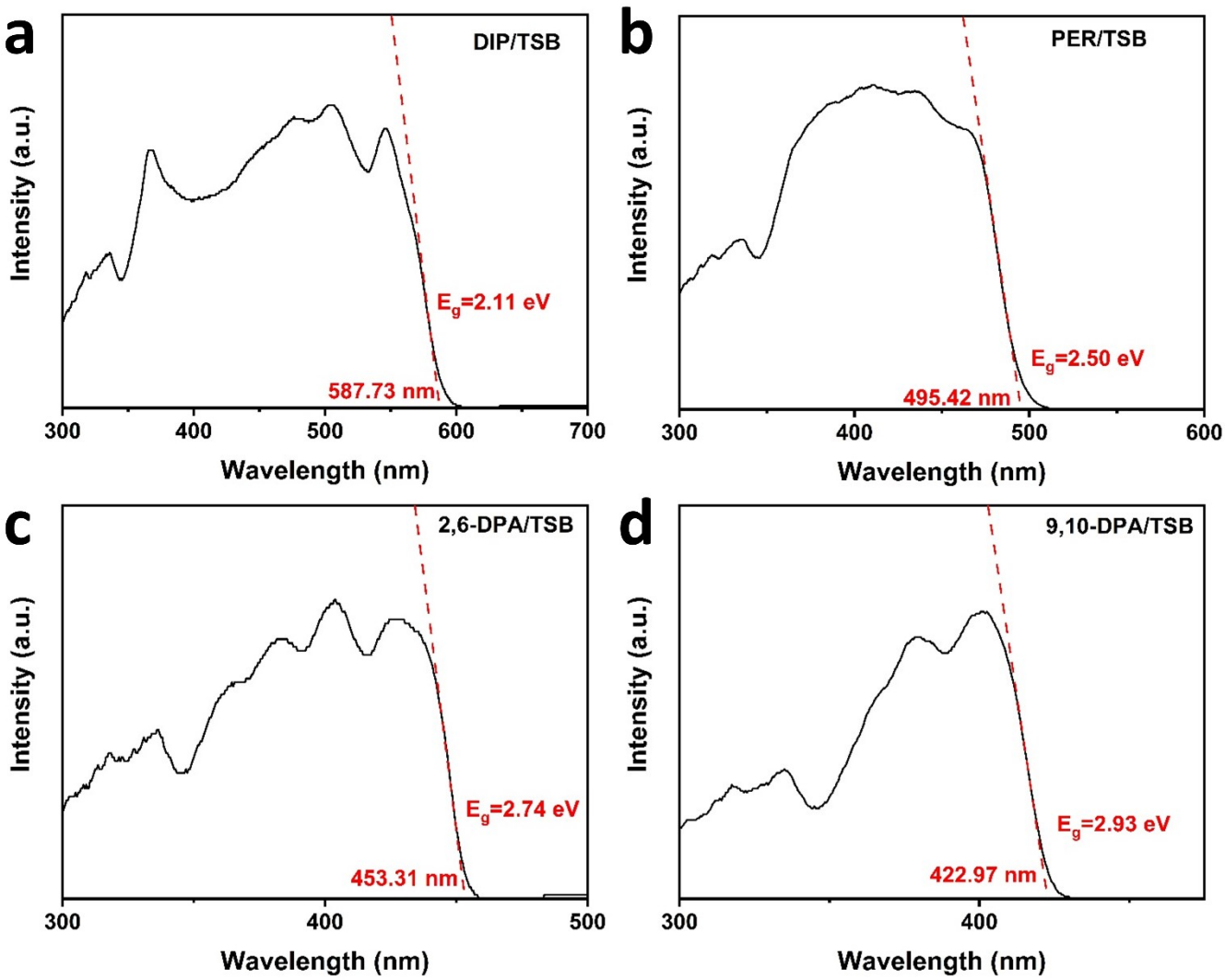

Figure S8. Band gaps of the four doped crystals estimated using UV-Vis absorption spectroscopy.

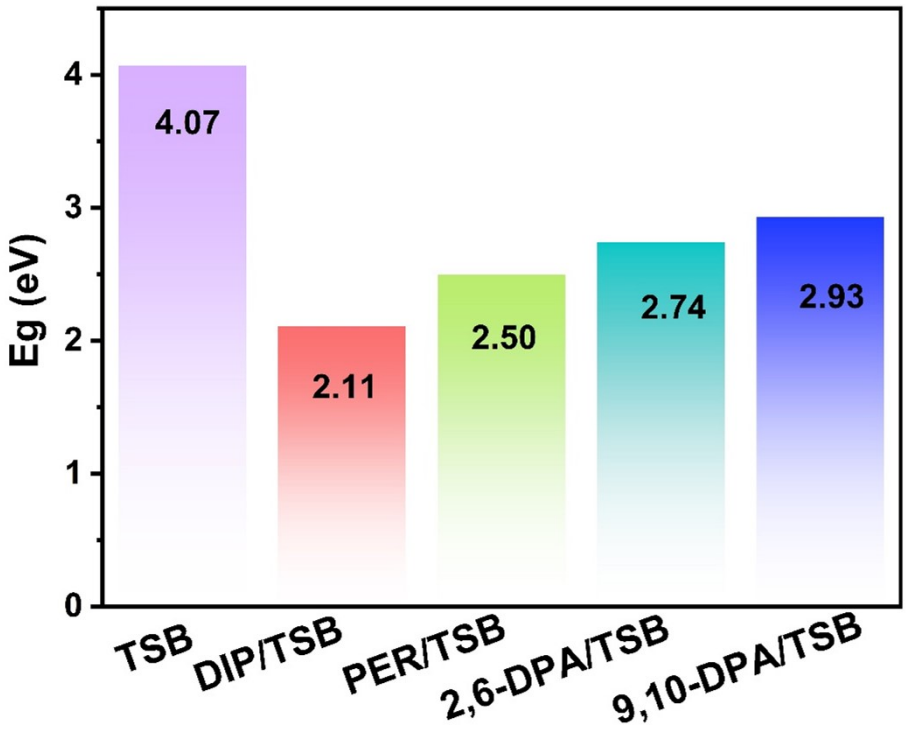

Figure S9. Bandgap comparison of TSB, DIP/TSB, PER/TSB, 2,6-DPA/TSB, and 9,10-DPA/TSB crystals.

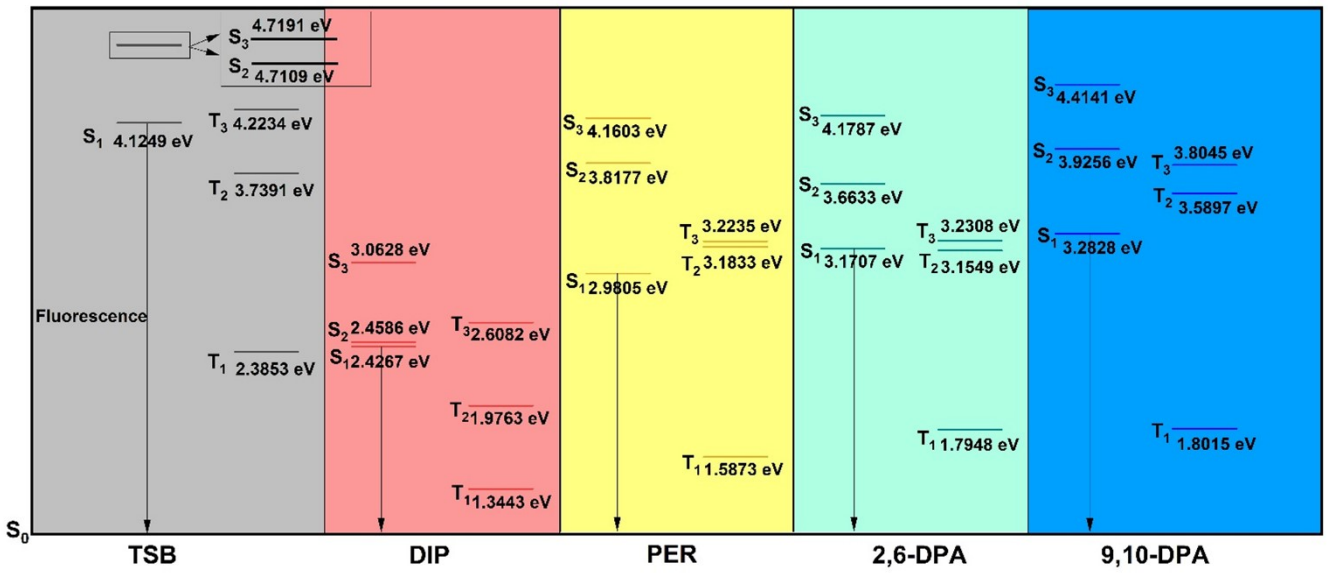

Figure S10. Singlet-Triplet Energy Level Diagram of TSB, DIP, PER, 2,6-DPA, and 9,10-DPA Molecules.

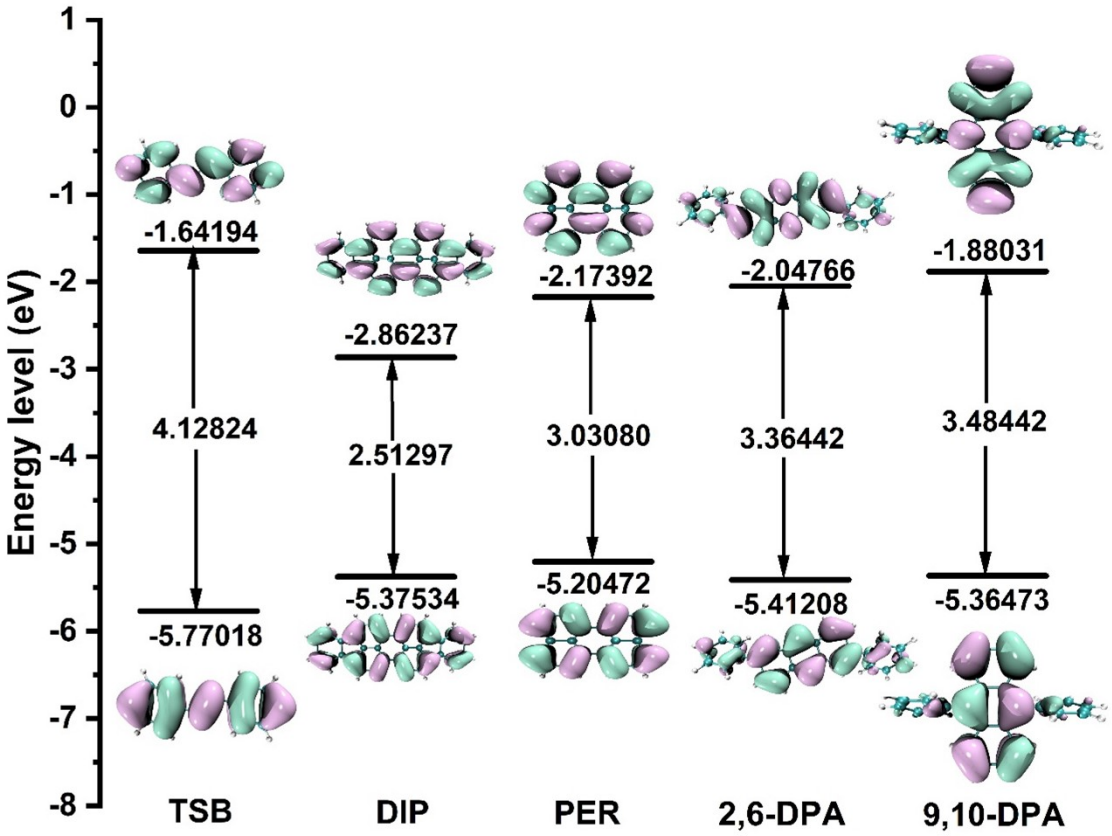

Figure S11. The optimized configurations, energy levels, and contours of the frontier molecular orbitals based on single-crystal diffraction data.

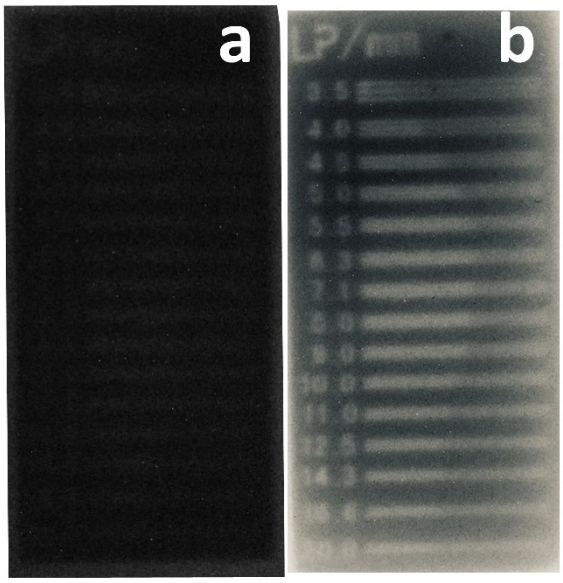

Figure S12. X-ray exposure contrast images of the line-pair card (Type 25N: 3.5–20 lp/mm) obtained using (a) TSB and (b) 2,6-DPA/TSB as scintillator films.

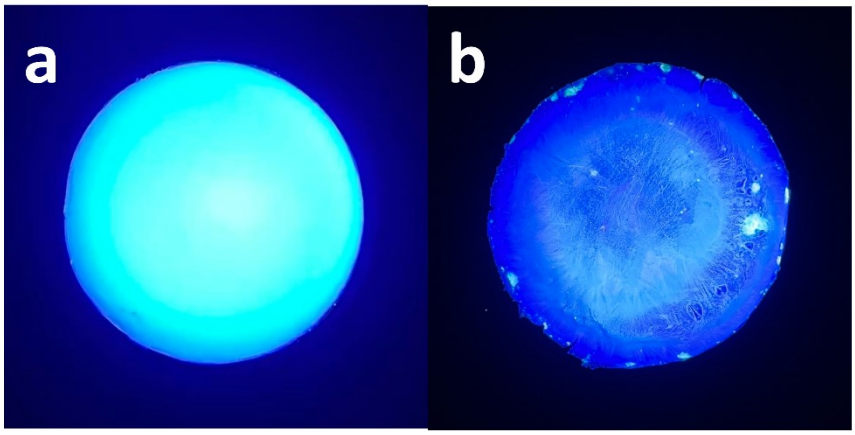

Figure S13. Comparative images of imaging polymer films prepared from (a) crystal powder of 2,6-DPA/TSB grown by the melt method and (b) a physical mixture of TSB and 2,6-DPA at the same molar ratio.

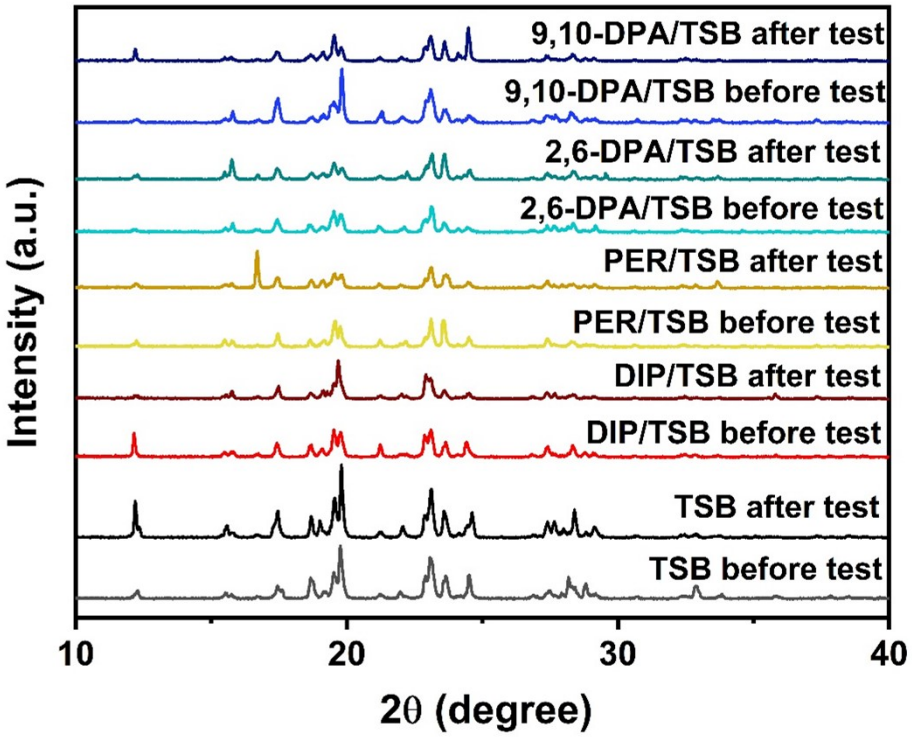

Figure S14. Comparative analysis of X-ray Diffraction patterns for TSB, DIP/TSB, PER/TSB, 2,6-DPA/TSB, and 9,10-DPA/TSB samples before and after radiation testing.

Table S1. The X-ray dose rate versus voltage/current.

Current (μA)	Voltage (kV)	Dose rate (μGy s^{-1})
5	30	9.64
5	40	11.91
5	50	17.38
10	50	34.75
20	50	69.50
30	50	104.25
40	50	139.00
50	50	173.75
60	50	208.50
70	50	243.25
80	50	278.00